Geo-Mar Lett (2014) 34:297–314
DOI 10.1007/s00367-014-0370-6

ORIGINAL

Geoacoustic character, sedimentology and chronology of a cross-shelf Holocene sediment deposit off Cabo Frio, Brazil (southwest Atlantic Ocean)

Ursula Mendoza · Arthur Ayres Neto · Rodrigo C. Abuchacra · Cátia Fernandes Barbosa · Alberto G. Figueiredo Jr. · Manoela C. Gomes · Andre L. Belem · Ramsés Capilla · Ana Luiza S. Albuquerque

Received: 2 October 2013 / Accepted: 25 March 2014 / Published online: 22 April 2014

Abstract The Cabo Frio region in the state of Rio de Janeiro, southeast coast of Brazil, is characterized by a local coastal upwelling system and converging littoral sediment transport systems that are deflected offshore at Cabo Frio, as a consequence of which a thick cross-shelf sediment deposit has developed over time. To investigate the evolution of this muddy deposit, geophysical, sedimentological and geochemical data from four sediment cores (3.8–4.1 m in length) recovered in water depths between 88 and 141 m were analyzed. The high-resolution seismic data show variable sediment thicknesses ranging from 1 to 20 m, comprising two sedimentary units separated by a high-impedance layer at a depth of about 10 m below the seafloor at the coring sites. According to the available age datings, the upper sedimentary unit is late Pleistocene to Holocene in age, whereas the lower unit (not dated) must, by implication, be entirely Pleistocene in age. The boomer-seismic reflection signal can be divided into three echo-types, namely *transparent* (inner shelf), *stratified* (middle shelf) and *reflective* (outer shelf), each type seemingly related to the local sediment composition. The upper 4 m of the upper sedimentary unit is dominated by silty sediment on the middle shelf, and by upward-fining sediments (silty sand to sandy silt) on the inner and outer shelf. The downcore trends of P-wave velocity, gamma-ray density and acoustic impedance are largely similar, but generally reversed to those of water and organic carbon contents. Total organic carbon contents increase with decreasing mean grain size, periodic fluctuations suggesting temporal changes in the regional hydrodynamics and primary productivity fuelled by the local upwelling system. The reconstruction of sedimentation rates in the course of the Holocene is based on 35 AMS age datings of organic material recovered from variable downcore depths. These range from a maximum of 13.3 cm/decade near the base of the inner shelf core (7.73–7.70 ka BP) to generally very low values (<0.11 cm/century) over the last thousand years in all cores. Over the last 6 ka there appear to have been three distinct sedimentation peaks, one between 6 and 5 ka BP, another between 4 and 3 ka PB, and one around 1 ka BP. Due to different time intervals between dates, not every peak is equally well resolved in all four cores. Based on the similar sedimentology of the inner and outer shelf cores, an essentially identical sedimentation model is proposed to have been active in both cases, albeit at different times. Thus, already during the last glacial maximum, alongshore sediment transport was deflected offshore by a change in shoreline orientation caused by the Cabo Frio structural high. The source of terrigenous material was probably a barrier-island complex that was subsequently displaced landward in the course of sea-level rise until it stabilized some 6.5 ka BP along the modern coast.

U. Mendoza · C. Fernandes Barbosa · A. L. Belem · A. L. S. Albuquerque (✉)
Departamento de Geoquímica, Instituto de Química, Universidade Federal Fluminense, 24020-150 Niterói, RJ, Brazil
e-mail: ana_albuquerque@id.uff.br

A. Ayres Neto · R. C. Abuchacra · A. G. Figueiredo Jr. · M. C. Gomes
Departamento de Geologia, Instituto de Geociências, Universidade Federal Fluminense, 24210-346 Niterói, RJ, Brazil

R. Capilla
Petrobras/Cenpes/Geoquímica, Cidade Universitária, Ilha do Fundão, 21941-915 Rio de Janeiro, Brazil

Introduction

The acoustic characteristics and physical properties of sediments are important variables sensitive to geological events

that may be preserved in the sedimentary record of continental shelf deposits. The intrinsic capacity of sediments to differentially absorb and scatter sound waves enables the acoustic classification and discrimination of sedimentary facies, and their distinction from underlying rocks and buried objects (e.g., Briggs et al. 2002). Already during the late 1960s, seabed echo characteristics were explored as a means to interpret late Quaternary sedimentation processes in various settings worldwide, including the southeastern continental shelf of Brazil (for an overview, see Damuth and Hayes 1977). Indeed, high-resolution seismic data have long served to identify geomorphological features characterized by key sedimentary processes (e.g., Damuth 1975; Damuth and Hayes 1977; Manley and Flood 1989; Hong and Chen 2000). For example, Davis et al. (2002) derived surficial seabed sediment properties based on seismic reflection characteristics in the Clyde Sea and the southern Baltic Sea, which were then used to interpret complex interrelationships between the geological setting, sediment supply, prevailing winds, oceanographic and paleoclimatic conditions, and sea-level fluctuations. Another well-known proxy is sediment organic matter (e.g., Flemming and Delafontaine 2000; Omura and Hoyanagi 2004; Sanders et al. 2014).

In this context, the Cabo Frio upwelling system, which is located on the southeastern Brazilian continental shelf, can be regarded as a natural laboratory to explore relationships between sedimentary processes and geophysical sediment characteristics. This site has been influenced by the oligotrophic Brazil Current, wind-induced coastal Ekman transport, sea-level changes and associated climatic oscillations during the late Pleistocene–Holocene (e.g., Angulo and Lessa 1997). Thus, a mid-Holocene sea-level highstand was followed by a series of sea-level oscillations of several meters that occurred over a few thousand years before stabilizing at approximately the present-day level. These variations resulted in a predominance of terrigenous sediment on the inner shelf, and bioclastic carbonate sediment on the outer shelf (Figueiredo Jr and Madureira 2004).

The Cabo Frio region (cf. Fig. 1), where northward- and southward-flowing wind-driven littoral currents converge, displays an extensive accumulation of muddy sediment that is oriented normal to the modern shoreline and reaches almost to the outer continental shelf. This elongated, cross-shelf muddy deposit was initially described by Kowsmann and Costa (1979) and Dias et al. (1982). More recent studies in the wider region focused on physical, geochemical, sedimentological and paleoceanographic aspects of the area (e.g., Mahiques et al. 2002, 2004, 2005, 2009, 2011; Nagai et al. 2009; Gyllencreutz et al. 2010; Souto et al. 2011; Cruz et al. 2013), whereas high-resolution shallow seismic surveys and coring operations aimed at a better understanding of the stratigraphy and acoustic properties of the seafloor in the region surrounding Cabo Frio Island were conducted by the Brazilian Navy (Artusi and Figueiredo 2007; Macedo et al. 2009). The area occupies a strategic position at the boundary between the Campos and Santos sedimentary basins, which are currently prime hydrocarbon exploration targets.

In the regional context outlined above, the aim of the present study was to unravel the Holocene sedimentological evolution of the Cabo Frio shelf by integrating variations in the echo character- and age-constrained downcore physico-chemical and geochemical parameters within the cross-shelf sediment deposit.

Physical setting

The Cabo Frio promontory marks a pronounced change in the orientation of the coastline from NE–SW north of the cape to E–W south of it (Fig. 1). The E–W portion of the coastline is exposed to SW–SE winds that are associated with cold fronts, whereas the NE–SW portion is typically exposed to NE–E winds.

Barrier island and lagoon systems are considered to be important indicators of the sedimentological history and coastline orientation in Brazil (e.g., Barbosa and Suguio 1999; Sallun et al. 2012). It can thus be assumed that this also applies to the Cabo Frio coastal area, where a large barrier island system has probably been present since the early Holocene because of the influence of the Cabo Frio High, which determines the present-day coastline orientation. The study area straddles the Cabo Frio structural high, which separates the Campos Basin to the north from the Santos Basin to the south. After the last glacial maximum (LGM), the Brazilian shelf experienced three phases of accelerated sea-level rise at approx. 11, 9, and 8 ka BP (Kowsmann and Costa 1979; Corrêa 1996; Sawakuchi et al. 2009). Barbosa (1997) identified two highstand/stillstand (H/S) phases in the sedimentary succession of the nearby Lagoa Vermelha at 5.1 ka BP and at approx. 0.75 ka BP.

The oceanography of the Cabo Frio continental shelf is complex. The Brazil Current (BC), which is a southward-flowing western boundary current, mainly follows the 100–200 m isobaths (Castro and Miranda 1998; Viana et al. 1998), but meanders of the current frequently approach the shelf and facilitate intrusions of South Atlantic Central Water onto the shelf. This water upwells along the coast in response to the prevailing northeasterly winds (Castelao and Barth 2006). The dynamics of these wind-driven nearshore currents are controlled by seasonal meteorological forcing. Due to the change in shoreline orientation and the presence of the protruding cape, the interaction between the dominant wind field and the seafloor topography is the main cause of the coastal upwelling, which is intensified during the austral summer in response to the South Atlantic high pressure cell (Rodrigues and Lorenzzetti 2001; Franchito et al. 2008).

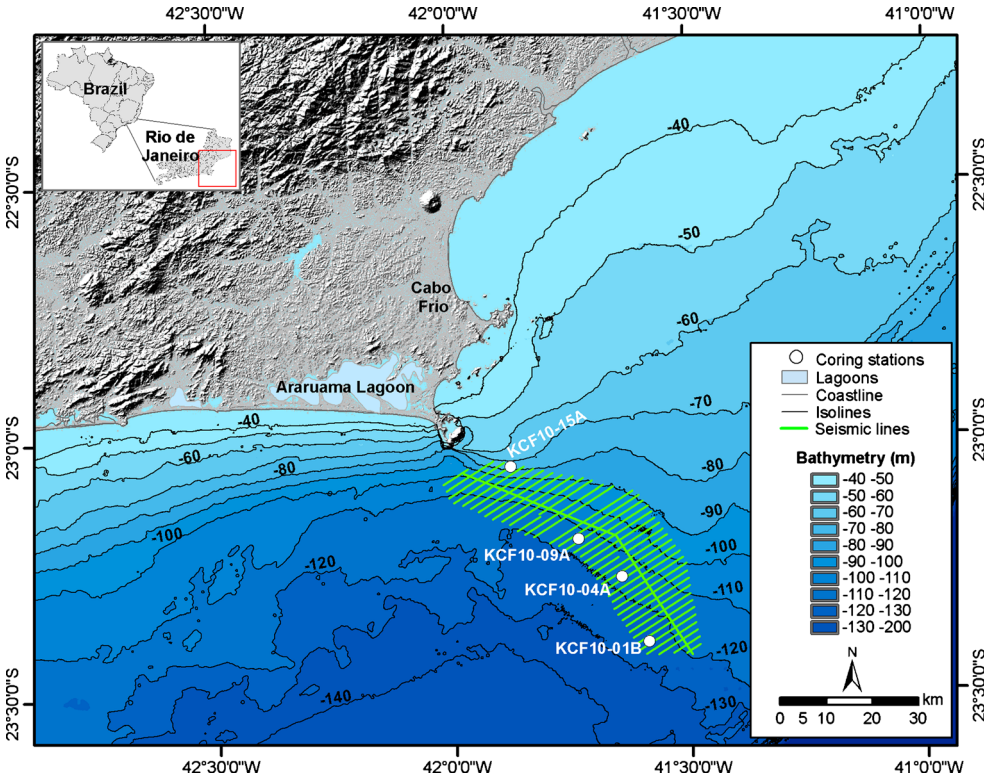

Fig. 1 Map of the study area off Cabo Frio showing the bathymetry, the locations of the seismic survey lines and coring sites, and the onshore topography and coastal lagoons. Notations: WGS84 datum

Sediment transport patterns on the inner shelf are controlled by wind-driven circulation (NE trade winds), whereas sediment dispersal on the outer shelf follows the meandering motion of the Brazil Current (Mahiques et al. 2002). However, the flow on the mid-shelf is primarily controlled by cross-shelf currents that are driven by the intensity of upwelling along the coast and tidal currents (Belem et al. 2013). Sediment is supplied by local rivers, including the Paraiba River, which is located about 180 km north of Cabo Frio, and Guanabara Bay, which is located 150 km west of the cape (Knoppers and Moreira 1990).

Materials and methods

Bathymetric and seismic data

Bathymetric and seismic data, as well as four piston cores (cf. below), were collected from aboard the RV *Ocean Survey* at the end of 2009 and the beginning of 2010 (Fig. 1). Navigation was controlled by a differential global positioning system with an accuracy of ~1 m (WGS84 datum). The high-resolution seismic/bathymetric survey covered an area of 680 km^2 along a cross-shelf section of approx. 40 nautical miles, comprising 42 SE–NW- and NE–SW-aligned profiles ranging in length from 3 to 21 km and spaced at 1.5 km intervals (Fig. 1). In addition, two 30- and 35-km-long SE–NW tie lines were run through the central part of the study area.

The bathymetric data were recorded by means of a 300 kHz Simrad EM3000 dual-head multibeam echosounder. The raw data were corrected for varying tidal elevations using the tidal harmonic constants for Arraial do Cabo (Cabo Frio) obtained from the tide tables of the Diretoria de Hidrografia e Navegação (DHN, Rio de Janeiro). The geophysical survey included seismic profiling employing a 3.5 kHz GeoPulse™ boomer (GeoAcoustics Ltd., Great Yarmouth, UK). A constant sonic velocity of 1,550 m s^{-1} was selected to depth-convert the seismic travel times; this corresponds to the average P-wave velocity measured in the cores.

Piston cores

To track potential interrelationships between seismic echo characters and various physical sediment properties in inner and outer shelf sediments, four cores (3.8–4.0 m in length) were collected at water depths of 88, 110, 112 and 141 m using a 6-m-long and 10-cm-diameter piston corer fitted with a 750 kg weight unit. The precise locations of the coring sites are provided in Fig. 1 and Table 1. The cores were stored horizontally onboard the ship at 4 °C. In the laboratory, P-wave velocity (Vp) and gamma-ray density were measured at 1 cm intervals using a GEOTEK multi-sensor core logger. Downcore acoustic impedance was calculated as the product of these two parameters.

After scanning, the sediment cores were sampled at 5 cm intervals. Absolute water contents were determined by oven

Table 1 AMS radiocarbon ages of organic matter. *Asterisks* Radiocarbon dating inversions (NB: these ages were omitted from Figs. 5 and 8)

Code	Core depth	^{14}C age	Calibrated age in calendar years (2σ)		
	(cm)	(ka BP)	Minimum	Cal. year BP	Maximum
Core CF10-01B: 23°24′ 14′ ′ S, 41°35′ 27′ ′ W, water depth 141 m					
AA93441	1	1.03–36	628	675	775
AA93442	21	1.72–38	1,174	1,270	1,347
AA89728	40	2.96–48	2,580	2,730	2,849
AA90736	80	3.45–41	3,205	3,330	3,430
AA93445	131	4.05–39	3,936	4,080	4,218
AA90738	140	4.94–44	5,110	5,280	5,430
AA93447	171	5.73–41	6,001	6,170	6,252
AA90734	200	6.99–48	7,400	7,475	7,570
AA93448	211	6.59–43	6,977*	7,135*	7,228*
AA93449	231	8.80–48	9,357	9,470	9,548
AA89729	250	10.86–59	10,868*	11,110*	11,190*
AA90735	300	9.25–56	9,885*	10,130*	10,210*
AA90739	340	9.05–67	9,530	9,730	10,010
AA93451	361	9.27–50	9,913	10,140	10,212
AA89730	370	11.1–110	12,363	12,620	12,886
Core CF10-04A: 23°16′ 36′ ′ S, 41°38′ 44′ ′ W, water depth 112 m					
AA89734	9	2.25–39	1,722	1,860	1,955
AA90184	51	2.73–39	2,316	2,420	2,606
AA90185	151	4.25–42	4,206	4,370	4,491
AA89735	205	4.94–42	5,109	5,280	5,423
AA90187	351	5.84–46	6,159	6,260	6,376
AA89736	392	6.97–44	7,391	7,460	7,560
Core CF10-09A: 23°12′ 05′ ′ S, 41°44′ 13′ ′ W, water depth 110 m					
AA90188	1	1.36–37	784	910	993
AA89740	10	1.92–48	1,335	1,480	1,590
AA90190	71	2.76–45	2,336	2,460	2,653
AA90192	131	3.18–40	2,836	2,960	3,117
AA90193	161	3.55–41	3,329	3,420	3,549
AA90194	251	4.43–42	4,434	4,570	4,733
AA90195	281	4.89–43	5,033	5,250	5,309
AA90197	341	5.38–45	5,624	5,730	5,874
AA89742	399	6.63–42	7,020	7,150	7,260
Core CF10-15A: 23°03′ 31′ ′ S, 41°52′ 37′ ′, water depth 88 m					
AA89746	34	1.09–39	550	650	714
AA89743	60	3.11–38	2,759	2,860	2,998
AA90731	100	7.26–60	7,590*	7,710*	7,855*
AA90744	160	5.13–55	5,322	5,470	5,585
AA90732	200	6.59–60	6,940	7,140	7,241
AA90745	260	6.67–54	7,034	7,220	7,318
AA89747	298	6.87–42	7,280	7,400	7,470
AA89742	340	7.27–46	7,612	7,700	7,836
AA90733	380	7.28–58	7,605	7,730	7,870

drying aliquots of bulk sediments at 60 °C, without correction for salt contents. After removal of carbonate by acidification with 1 mol HCl, total organic carbon (TOC) content was measured on other aliquots by means of a PDZ Europa ANCA-GSL elemental analyzer at the Davis Stable Isotope Facility, University of California, CA.

For grain-size analyses, fresh sediment samples (2 g) were oven dried at 105 °C after carbonate had been removed by treatment with 1 mol HCl. Grain-size distributions at 0.5 phi intervals of the <500 μm fractions were generated using a Cilas® 1064 laser grain-size analyzer. Statistical parameters were determined based on the Gradistat routine of Blott and Pye (2001), and the textural data were derived using the method of moments (cf. Swan et al. 1979; Krumbein and Pettijohn 1988; Blott and Pye 2001; Sawakuchi et al. 2009). Downcore sediment descriptions are based on mean grain size and sand/silt/clay contents (cf. modified Wentworth scale, Krumbein and Pettijohn 1988).

Downcore chronology was determined by AMS radiocarbon dating of carbonate-free organic matter in 39 samples at the NSF Radiocarbon Laboratory, University of Arizona, Tucson, AZ (Table 1). Sediments were decarbonated using 1 mol HCl, the $\delta^{13}C$ values of –21 to –24‰ indicating that the samples were carbonate-free. The radiocarbon ages were calibrated based on the Calib 6.0 software of Stuiver et al. (1998) and specifically the Marine09 curve, which considers intervals between 2σ and a southwest Atlantic reservoir effect of $\Delta R=8 \pm 17$ years (Angulo et al. 2005). The calibrated age (single value) represents the maximum probability within the 2-sigma range. These data enabled the calculation of sedimentation rates for successive age intervals. Because the age intervals vary along the cores and between cores, the calculated sedimentation rates (expressed as cm/century) must be considered as average values for the corresponding age intervals.

Interrelationships between various physical and geochemical parameters were evaluated based on the Pearson correlation coefficient at 95% confidence intervals, using the Microsoft Statistica 8.0 statistical software package. Correlations <0.6 are considered as weak, and those >0.6 as strong (Anderson and Finn 1996).

Results

Only one laterally extensive high-impedance reflector was identified on the seismic profiles. This reflector is considered to represent the interface between two distinct sedimentary units. Because none of the 4-m-long cores penetrated into the lower unit or even to the interface, only the top 4 m of the upper unit are discussed here. Seeing that the ages near the base of the cores range from approx. 12.6 to 7.3 ka BP, however, the lower sedimentary unit must, by implication, be entirely of Pleistocene age, whereas the upper unit comprises both late Pleistocene and Holocene sediments (cf. below).

Seismic profiles

The acoustic character of the seismic profiles can be subdivided into three major echo-types: transparent, stratified, and reflective (Fig. 2). The *transparent* echo-type characterizes the deposits on the outer shelf where core KCF10-01B was collected. Here, the seismic records are completely transparent with the exception of a single, sharply defined high-impedance reflector interpreted to separate an upper and lower sedimentary unit (Fig. 2a).

The *stratified* echo-type characterizes the deposits of the central sector represented by cores KCF10-04A and KCF10-09A. Here, the seismic records reveal a sequence of discontinuous parallel reflections that are interrupted by a single continuous and more sharply defined reflector of higher impedance, interpreted to represent the boundary between the upper and lower sedimentary unit (Fig. 2b).

The *reflective* echo-type, characterized by a reflective seabed without internal seismic reflections, is observed in the northwestern sector where it is represented by the seismic line crossing core site KCF10-15A on the inner shelf. This echo-type is similar to the transparent one, except that the seabed reflector is sharper (higher impedance) and the sub-bottom has a higher acoustic noise level that fades with depth without showing internal reflections of any kind (Fig. 2c).

The high-resolution seismic survey also revealed a NW–SE-oriented linear, approx. 6-km-long feature that outcrops about 2 m above the surrounding seafloor. This feature is located along the 110 m isobath between cores KCF10-09A and KCF10-04A (Fig. 3), and was recently identified as representing a low beach-rock ridge by Petrocelli (2013).

Sediment thickness

The thickest part of the upper sedimentary unit (20 m) is located in the northwestern part of the study area, where it appears to merge with or form the lower part of the modern shoreface at water depths of 90–100 m (Fig. 4). From here, the thickness of the unit initially decreases strongly southeastward across the shelf to 7 m (at ca. 100 m water depth), then increases to approx. 10 m before decreasing to <8 m in the central sector of the deposit. From this depositional low, the unit gradually thickens offshore to a maximum of 12 m northeast of the outer mid-shelf coring site (KCF10-04A). From this point southward to approx. 700 m northwest of the outer shelf coring site (KFC10-01B), the unit thins to <9 m and then thickens to >10 m halfway to the outer shelf coring site. The upper unit gradually thins from this location across the coring site to the outer shelf.

With the exception of the northernmost part, the upper unit thins to <2 m both to the northeast and the southwest of the center line. In contrast to the approximately symmetrical lateral thinning of most of the deposit, the sediment thickness pattern is asymmetrical along its thickest part in the central sector northeast of coring site KCF10-04A (Fig. 4). Here, the deposit progressively thickens toward the northeast before

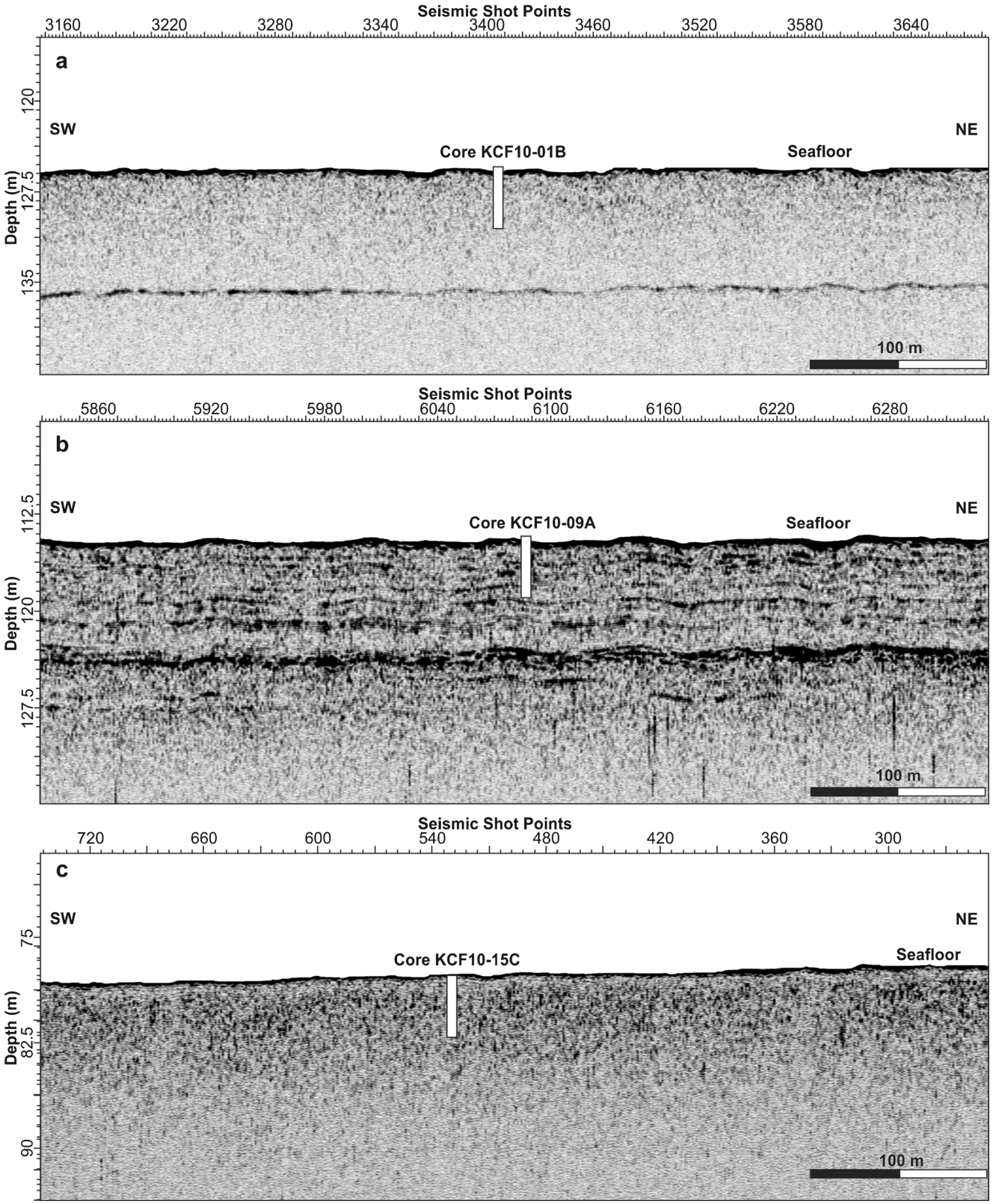

Fig. 2 Seismic sections illustrating the three echo-types identified in the study area: **a** transparent, **b** stratified, and **c** reflective. The examples cross three of the coring sites

strongly thinning from >12 m to about 6 m along a NW–SE-trending axis, which the seismic data show to be a ridge composed of beach rock (Fig. 3). The thinning of the sediment is probably controlled by structural features related to

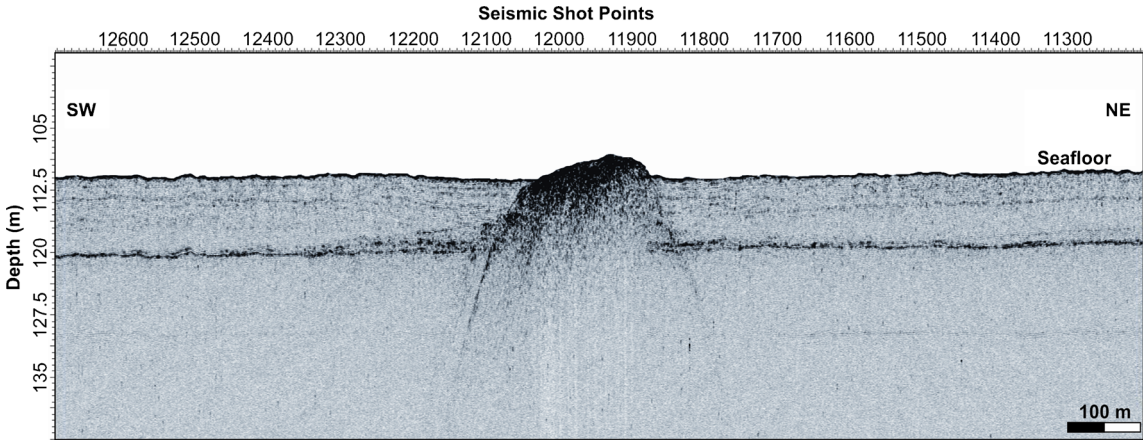

Fig. 3 Characteristics of seismic echoes in the vicinity of a NW–SE-aligned linear beach rock on the mid-shelf northeast of coring site KCF10-04A

the Cabo Frio High, which existed long before any mud accumulated.

Core descriptions

Core KCF10-01B

Core KCF10-01B was collected on the outer shelf at a water depth of 141 m and has a total length of 380 cm. The sediment composition varies progressively, though not uniformly, from approx. 92% sand, 8% silt and 0% clay (slightly muddy sand) near the base to approx. 40% sand, 53% silt and 7% clay (sandy mud) at the top (Fig. 5a). The transition from sand- to mud-dominated sediment occurs at a core depth of ca. 180 cm. The P-wave velocity, gamma-ray density and acoustic impedance have very similar trends; they all show relatively high values at the core base, which remain more or less constant to a depth of 240 cm (~9.4 cal. ka BP) before progressively

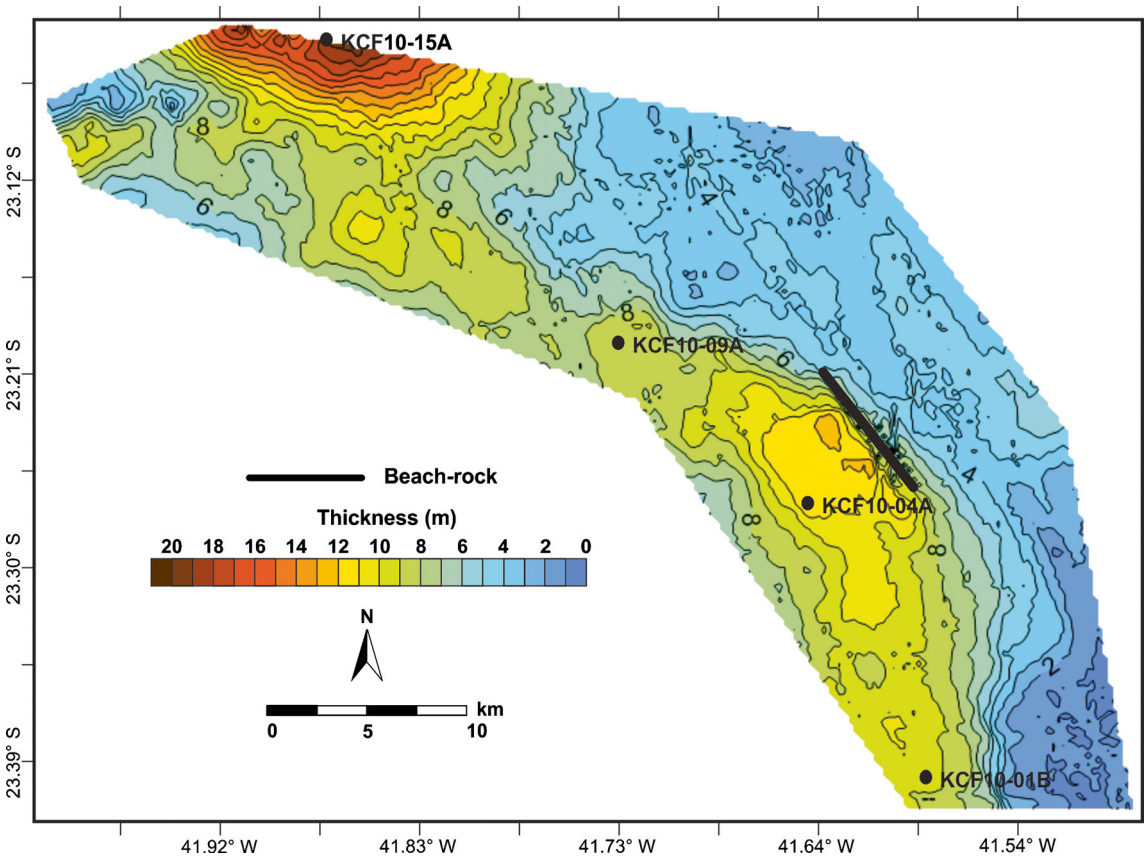

Fig. 4 Isopach map showing the thickness distribution of the upper sedimentary unit with the coring locations. Note the NW–SE-oriented beach rock northeast of coring site KCF10-04A. Notations: WGS84 datum

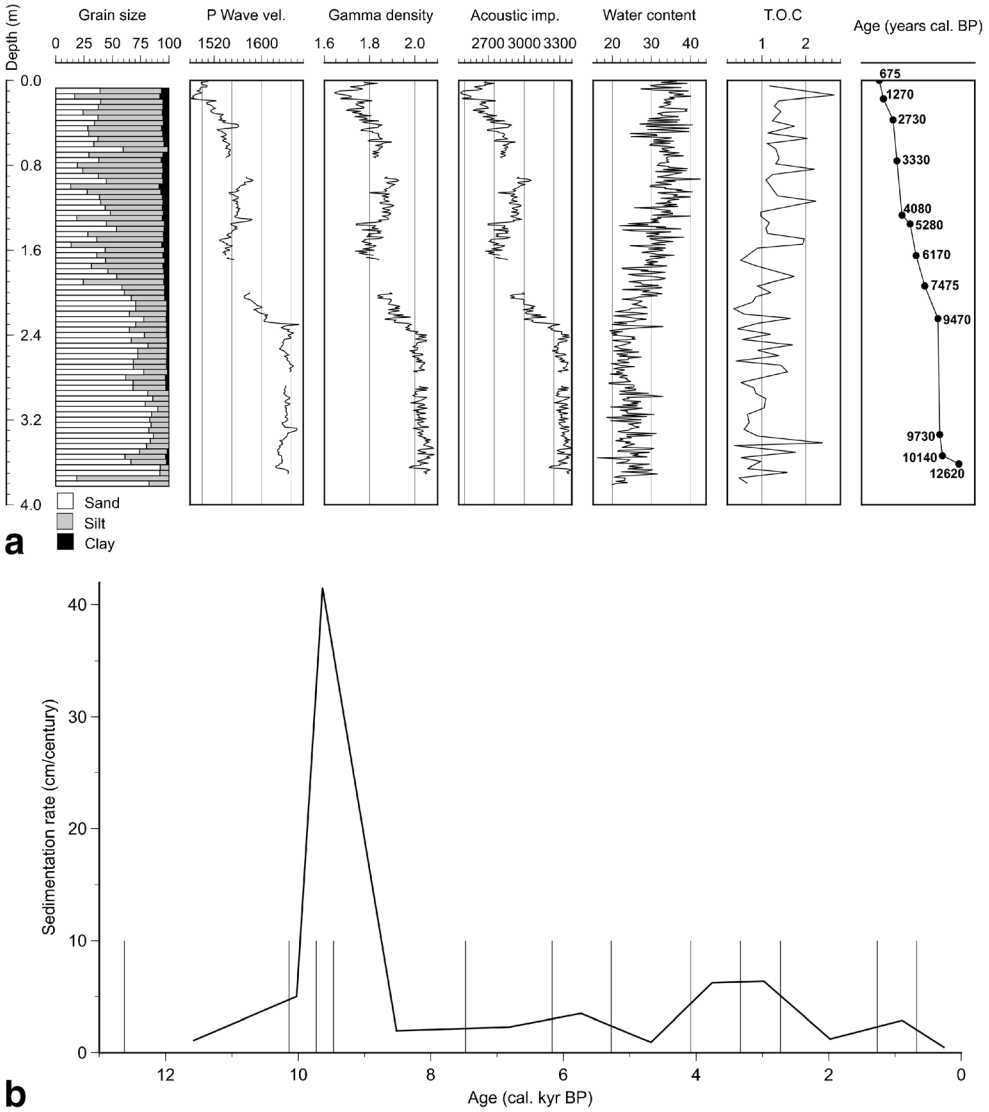

Fig. 5 **a** Downcore profiles for core KCF10-01B (141 m water depth): sand/silt/clay contents (%), P-wave velocity (m s^{-1}), gamma-ray density (g cm^{-3}), acoustic impedance (N s m^{-3}), water content (%), total organic carbon (TOC, %), and ages (cal. years BP). **b** Sedimentation rates over time. *Blue line* Mid-points of individual age intervals, *vertical gray lines* time slices for which AMS ages are available

decreasing up to a depth of 160 cm. The values then increase slightly to a core depth of about 90 cm, and then decrease; the lowest values are reached approx. 16 cm from the core top. Overall, the P-wave velocity varies from 1,520 to 1,763 m s^{-1}, the gamma-ray density from 1.6 to 2.1 g cm^{-3}, and the acoustic impedance from 2,545 to 3,364 N s m^{-3}.

Water content ranges from 20 to 38%, and is low (<25%) near the core base (380–350 cm core depth; Fig. 5a). The values peak at 38% at approx. 340 cm depth, then decrease stepwise to <25% at 220 cm depth, and increase again upcore with slight fluctuations of 3–5% until they reach 35% at the top of the core. Overall, TOC values vary from 0.30 to 1.86%, generally increasing from the core base (~0.4%) to the core top (~1.6%) but fluctuating by more than 1% at almost regular depth intervals.

Of the four cores, core KCF10-01B covers the largest age range, beginning at 12,620 cal. years BP near the core base at 370 cm depth. Twelve ages were available to calculate sedimentation rates (Table 2). As illustrated in Fig. 5b, the oldest age interval has a very low sedimentation rate, which then increases and peaks at ~41.92 cm/century at 9,730–9,470 cal. years BP. Thereafter, the sedimentation rates remain low, although three minor peaks occur at 6,170–5,280, 4,080–2,730, and 1,270–675 cal. years BP. The top 1 cm of the core covers the past 675 years, associated with a very low sedimentation rate of 0.15 cm/century. Unfortunately, the high sedimentation rate on the outer shelf at the onset of the Holocene lies beyond the age range of the other three cores, which prevents a comparison with these other shelf sites.

Core KCF10-04A

Core KCF10-04A was collected on the outer mid-shelf at a water depth of 112 m and is 400 cm long. The sediment essentially consists of sandy to slightly sandy mud (Fig. 6a). The highest sand contents (up to 45%) occur in the lower part of the core (below 300 cm). Above that depth, the values vary between 0% and 25%, but generally decrease toward the core top. Clay contents fluctuate by approx. 10% in the lower part of the core (<300 cm depth). The values increase slightly to approx. 15% at ca. 148 cm core depth, followed by a sharp peak of 60% before decreasing again. From approx. 130 cm core depth to the core top, clay contents remain almost constant at about 5%. With the exception of the single clay-rich interval, the core material is thus dominated by silt-size sediment.

In contrast to the outer shelf core, only the gamma-ray density and acoustic impedance show similar trends; overall, the values are higher at the bottom of the core, and decrease to in the upper part (Fig. 6a). From the core base to approx. 300 cm depth, the two parameters show relatively stable high values, which then progressively decrease with considerable fluctuations toward the core top. The range in gamma-ray density is 1.66–1.87 g cm^{-3}, and that for impedance is 2,524–2,760 N s m^{-3}. The P-wave velocity, by contrast, is low at the base of the core (~1,496 m s^{-1}), and then steadily increases to a peak value of ~1,540 m s^{-1} at ca. 350 cm core depth, followed by a stepwise decrease to ~1,480 m s^{-1} at ca. 264 cm depth, and an increase to about 1,500 m s^{-1} at 235 cm depth. From that depth upcore, values fluctuate at 1,488–1,516 m s^{-1} up to a core depth of 80 cm, and then decrease to about 1,480 m s^{-1} in the uppermost part of the core.

Water content is low (approx. 38%) from the core base up to a core depth of 280 cm, where it reaches a minimum of 34%. It then overall increases to 56% near the top of the core, but fluctuating by up to 10%. The TOC content generally increases from approx. 1.8% near the core base to 3.11% at the core top, with strong spot variations of 0.75–3.11%; this maximum value is amongst the highest recorded at the two mid-shelf sites.

Core KCF10-04A covers the last 7,460 cal. years BP, with six ages available for calculation of sedimentation rates (Table 3). The oldest age interval has a relatively low sedimentation rate, which increases to peak strongly at 14.9 cm/century at 6,260–5,280 cal. years BP before decreasing again to 5.93 cm/century (Fig. 6b). A minor peak of 7.5 cm/century occurs at 2,420–1,860 cal. years BP. The sedimentation rate is very low in the youngest, uppermost part of the core.

Table 2 Sedimentation rates for age intervals in core KCF10-01B from the outer shelf

Age interval (cal. years BP)	Depth interval (m)	Sed. rate (cm/century)
0–675	0–1	0.15
675–1,270	1–21	3.36
1,270–2,730	21–40	1.50
2,730–3,330	40–80	6.67
3,330–4,080	80–131	6.80
4,080–5,280	131–140	0.75
5,280–6,170	140–171	3.48
6,170–7,475	171–200	2.22
7,475–9,470	200–231	1.55
9,470–9,730	231–340	41.92
9,730–10,140	340–361	5.12
10,140–12,620	361–370	0.36

Core KCF10-09A

Core KCF10-09A was collected on the inner mid-shelf at a water depth of 110 m, only 2 m shallower than the outer mid-shelf core site (cf. above). The core is 405 cm long. As in the case of the outer mid-shelf core, this core is dominated by silt; sediment composition gradually varies from slightly sandy mud (~18% sand content) at the core base to almost pure mud (<5% sand content) at the core top (Fig. 7a). There is a spot occurrence of an unusually high sand content of >90% about 25 cm above the core base at 380 cm core depth. Clay contents overall increase from approx. 10% near the core base to 25% at 80 cm depth, and then gradually decrease to 15% at the core top. There are only two spot occurrences of distinctly higher clay contents: 30% at 308 cm, and 50% at 132 cm core depth.

The P-wave velocity, gamma-ray density and acoustic impedance of the inner mid-shelf core have very similar trends: the values are overall high at the core base and low at the core top, albeit with some fluctuations (Fig. 7a). The range in P-wave velocity is 1,450–1,515 m s^{-1}, the corresponding values being 1.47–1.75 g cm^{-3} for gamma-ray density, and 2,134–2,650 N s m^{-3} for acoustic impedance. Water content varies from 37 to 57%, and increases toward the core top. This maximum value is the highest water content recorded for all cores combined; the next highest was found in the outer mid-shelf core (KCF10-04A, cf. above), in both cases associated with high mud contents. TOC contents also generally increase from the core base (~2.3%) to the core top (~3.2%), the fluctuations becoming weaker upcore. TOC values range from 1.33 to 3.27%.

Core KCF10-09A covers the last 7,150 cal. years BP, with nine ages available for calculation of sedimentation rates (Table 4). At the bottom of the core, the oldest age interval has a relatively low sedimentation rate of 4.08 cm/century, which then increases to peak distinctly at 12.5 cm/century at 5,730–5,250 cal. years BP (Fig. 7b). The values then decrease to approx. 4.41 cm/century before increasing to peak again between 3,460 and 2,960 cal. years BP. This is followed by

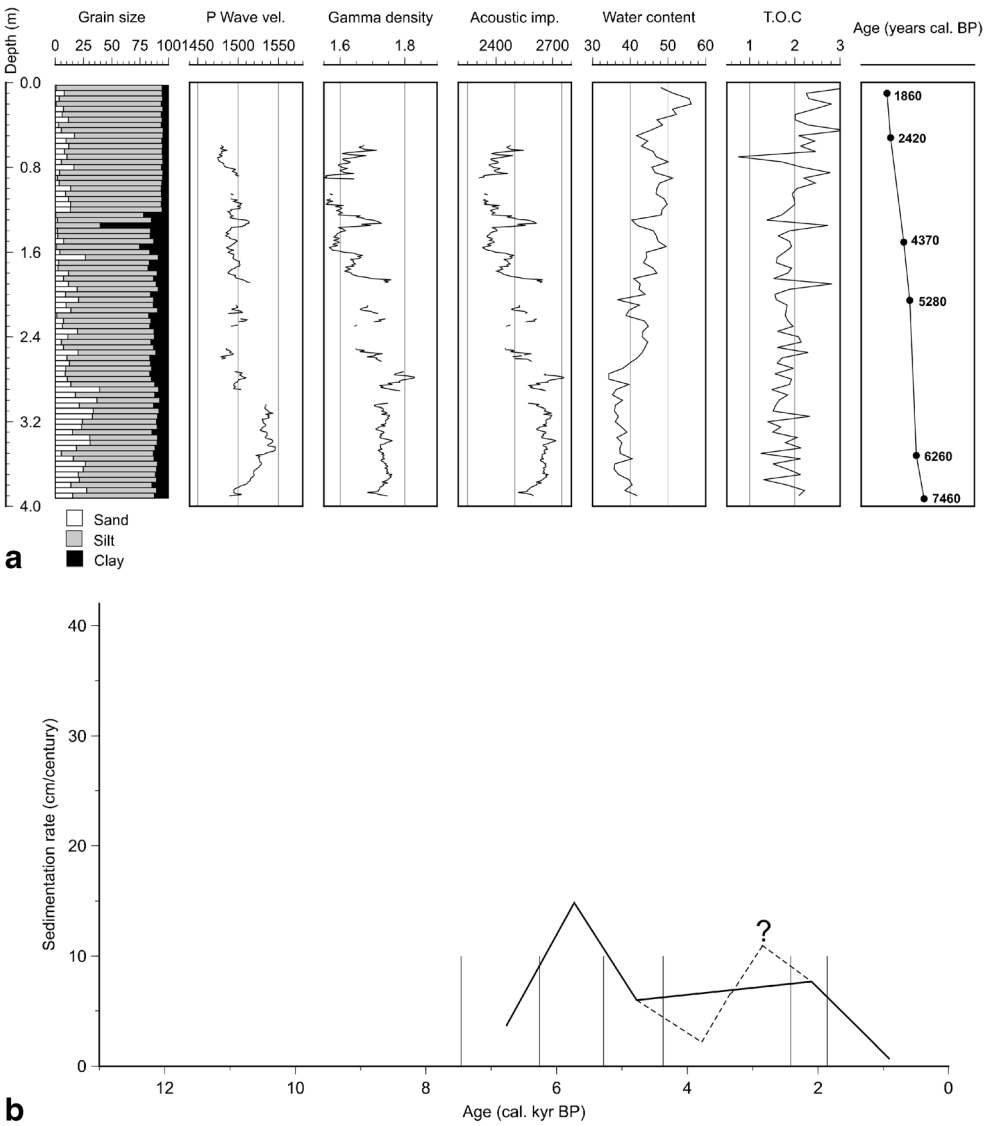

Fig. 6 **a** Downcore profiles for core KCF10-04A (112 m water depth): sand/silt/clay contents (%), P-wave velocity (m s^{-1}), gamma-ray density (g cm^{-3}), acoustic impedance (N s m^{-3}), water content (%), total organic carbon (TOC, %), and ages (cal. years BP). **b** Sedimentation rates over time. *Blue line* Mid-points of individual age intervals, *vertical gray lines* time slices for which AMS ages are available, *broken blue line* possible alternative trend if more closely spaced AMS ages were available from 2,420 to 4,370 cal. years BP

sedimentation rates progressively decreasing to a very low value of 0.11 cm/century in the youngest age interval in the uppermost part of the core.

Table 3 Sedimentation rates for age intervals in core KCF10-04A from the outer mid-shelf

Age interval (cal. years BP)	Depth interval (m)	Sed. rate (cm/century)
0–1,860	0–9	0.48
1,860–2,420	9–51	7.50
2,420–4,370	51–151	5.13
4,370–5,280	151–205	5.93
5,280–6,260	205–351	14.90
6,260–7,460	351–392	3.42

Core KCF10-15A

Core KCF10-15A was collected on the inner shelf at a water depth of 88 m and is 410 cm long. Sediment composition varies from slightly muddy sand at the core base (~80% sand, ~17% silt, ~3% clay) to sandy mud at the core top (~45% sand, ~50% silt, ~5% clay; Fig. 8a). Sand/mud contents generally fluctuate by approx. 10%, but locally by as much as 30% over short core intervals.

As in the other cores, P-wave velocity, gamma-ray density and acoustic impedance have very similar trends, varying from generally higher values at the core base to low values at the core top (Fig. 8a). The main difference with the other cores is that the values decrease more gradually up to a core depth interval of 50–30 cm, before decreasing sharply to very low values above this interval. In core KCF10-15A, the values of these three parameters increase slightly from the core base

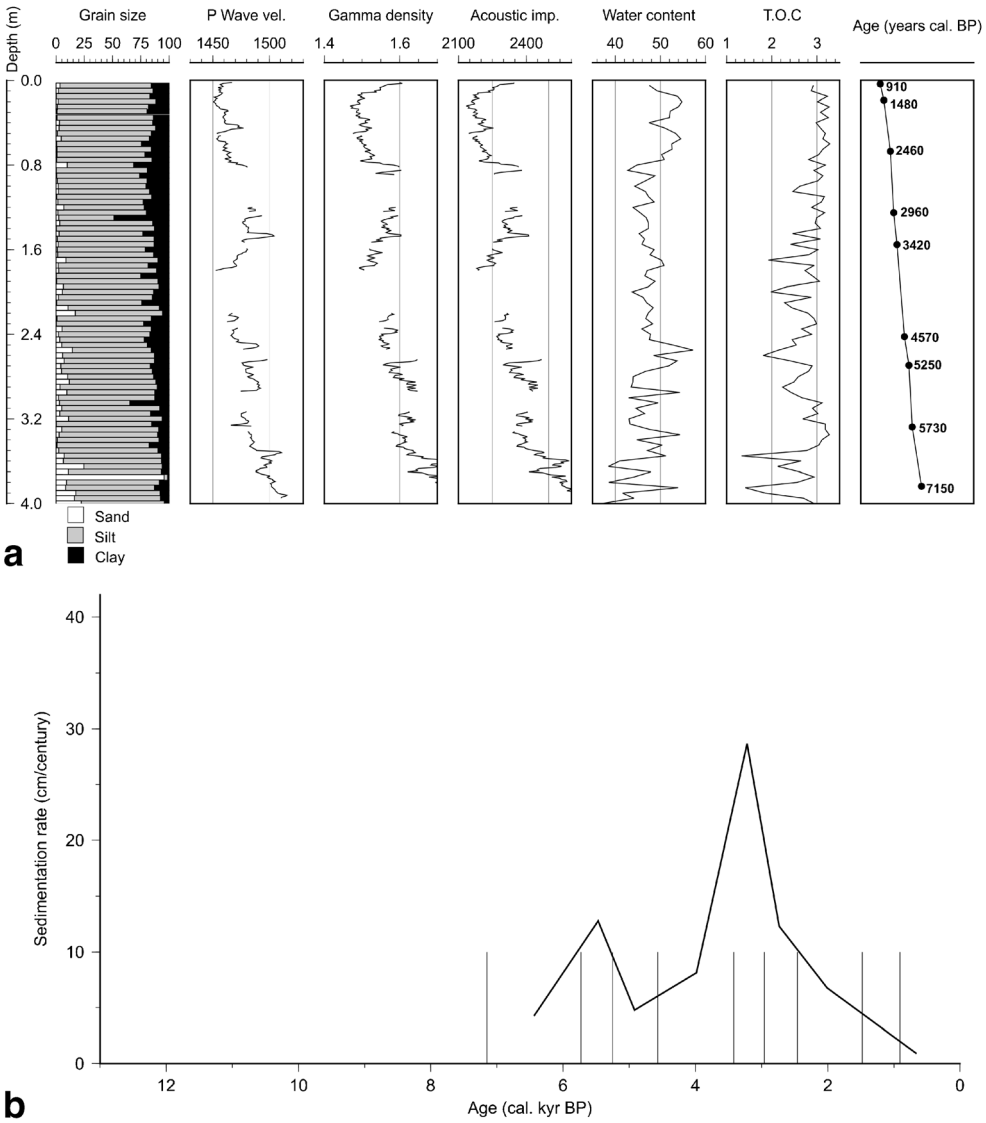

Fig. 7 **a** Downcore profiles for core KCF10-09A (110 m water depth): sand/silt/clay contents (%), P-wave velocity (m s^{-1}), gamma-ray density (g cm^{-3}), acoustic impedance (N s m^{-3}), water content (%), total organic carbon (TOC, %), and ages (cal. years BP). **b** Sedimentation rates over time. *Blue line* Mid-points of individual age intervals, *vertical gray lines* time slices for which AMS ages are available

up to depths of approx. 260 cm, and then decrease to intermediate values at core depths of approx. 100 cm. From that depth upcore, P-wave velocity increases up to a core depth of approx. 50 cm, and the other two parameters up to approx. 30 cm. All three parameters then decrease to reach their lowest values at the core top. The P-wave velocity ranges from 1,500–1,684 m s^{-1}, this maximum value being the highest recorded for all cores combined. Gamma-ray density is 1.55–2.0 g cm^{-3}, and acoustic impedance 2,194–3,358 N s m^{-3}. Water content increases from ~25% at the core base to ~40% at the core top, and fluctuates by as much as 5% over the range of 21–39%. TOC content increases progressively from ~0.8% at the core base to ~2.0% at the core top, varying from 0.16–2.13%.

Core KCF10-15A covers the last 7,700 cal. years BP, with eight ages available for sedimentation rate calculations (Table 5). In the lower half of the core, the five oldest ages cover a time period of only 590 years, but are associated with the highest sedimentation rates recorded at all four coring sites combined (Fig. 8b). The oldest, lowermost core interval (380–340 cm) extends from 7,730 to 7,700 cal. years BP, corresponding to an extrapolated peak sedimentation rate of 133.3 cm/century; indeed, more appropriate would be a rate of 13.3 cm/decade, because of the short time interval of only 30 years. The same argument applies to another sedimentation peak at 260 to 200 cm (40 cm interval) that extends from 7,220 to 7,140 cal. years BP (80 years), where the rate is more appropriately calculated as 5 cm/decade. The upper half of the core covers the remaining 7,140 years; the sedimentation rates vary from 1.17 to 5.23 cm/century, any shorter-period peaks being masked by the long time intervals between individual ages.

Age correlations between cores

When comparing sedimentation rates derived from unequal time intervals, the overall rates may obscure stronger

Table 4 Sedimentation rates for age intervals in core KCF10-09A from the inner mid-shelf

Age interval (cal. years BP)	Depth interval (m)	Sed. rate (cm/century)
0–910	0–1	0.11
910–1,480	1–10	1.57
1,480–2,460	10–71	6.22
2,460–2,960	71–131	12.00
2,960–3,420	131–161	28.26
3,420–4,570	161–251	7.83
4,570–5,250	251–281	4.41
5,250–5,730	281–341	12.50
5,730–7,150	341–399	4.08

fluctuations over shorter time intervals. Therefore, a synoptic chronostratigraphic cross-shelf diagram was constructed to link selected age intervals in the four cores relative to water depth. In Fig. 9, the spacing between any two successive isochrons (dashed blue lines) is proportional to the local sedimentation rates, whereas the sedimentation rates in adjacent intervals differ because of the different time periods. This diagram provides a good indication of the cross-shelf sedimentation trends in the study area over the past 7,000 years.

As already described above, only the outer shelf core (KCF10-01B) penetrated the entire Holocene succession. Figure 9 shows that the lowest sedimentation rate occurs on the outer shelf, and the next lowest on the inner shelf. Highest sedimentation occurs on the mid-shelf (cores KCF10-09A and KCF10-04A). Only the oldest age interval of the inner shelf (core KCF10-15A) shows a sedimentation rate similar to that of the mid-shelf. Of particular interest is the sudden decrease in sedimentation on the inner shelf between 2,860 and 1,000 cal. years BP, and the generally low rate over the past 1,000 years on the mid-shelf compared to the outer shelf and especially the inner shelf.

Statistical interrelationships

The Pearson correlation coefficients indicate a strong correlation between P-wave velocity and gamma-ray density (r=0.85); the former is also well correlated with mean grain size (r=–0.81). A very high correlation coefficient (r=0.87) exists between water content and mud content. Water content and TOC, by contrast, are weakly negatively correlated with sediment physical properties; for example, P-wave velocity versus TOC has a negative correlation of r=–0.24.

Discussion and conclusions

Sea-level history and physicochemical characteristics

To understand the complex sedimentary evolution of this area, three time slices were considered in the analysis. These describe well-known paleoenvironmental conditions around 12 and 6 ka BP, and the last 3 ka. It should be noted, however, that for pre-Holocene times the sea-level history of the Brazilian coast is still poorly understood.

During the last glacial maximum (ca. 18 ka BP) the relative sea level in the study area stood about 110 m below its present level and only the offshore coring site (KCF10-01B), located at a water depth of 141 m, was submerged at that time, the water depth being about 35 m. High-energy conditions in shallow water evidently allowed even coarse sand to be transported offshore up to and beyond the coring site. Two periods of rapid and sustained sea-level rise occurred from ca. 16 to 12.5 ka BP and again from ca. 11.5 to 8 ka BP (Fig. 10). These two phases of sea-level rise appear to be separated by the Younger Dryas, a period of global cessation of ice retreat (cf. Lambeck and Chappell 2001), sea level reaching about 60 m below the present-day one at 11.5 ka BP (cf. Guilderson et al. 2000; Tarasov and Peltier 2005). Straddling the Pleistocene–Holocene boundary (11.5 ka BP), these conditions persisted up to about 9.6 ka BP (Figs. 5a, 10) when relative sea level stood at about –40 m (Fig. 10; cf. Kowsmann and Costa 1979; Corrêa 1990; Guilderson et al. 2000; Artusi and Figueiredo 2007; Reis et al. 2013). In the course of sea-level rise, sand was thus initially deposited at all coring sites. As documented in Fig. 5a and b, maximum sedimentation rates occurred between about 10 and 8 ka BP. In correspondence, the Vp, gamma-ray density and acoustic impedance values are high (Fig. 5a). Only after 9.6 ka BP, when the water depth at the offshore coring site (KCF10-01B) was about 100 m, did the supply of sand to the outer shelf gradually decrease and the deposition of mud, especially of silt, increase.

Coring site KCF10-01B is located in the transparent echo domain, which Damuth (1975) interpreted as being caused by the presence of coarse sediment (sand or even gravel). As expected, average TOC content is low at the base of the core due to the high sand content, and increases toward the top with increasing mud content (Fig. 5a). The strong variations in TOC throughout the core could be evidence for corresponding climate fluctuations associated with changes in productivity. Such an interpretation is supported by the geochronological inversions observed in core KCF-10-01B (Table 1), which suggest that sea level fluctuated, especially around 7.8 and 6.7 ka BP (Corrêa 1996; Angulo and Lessa 1997; Bard et al. 1998; Tarasov and Peltier 2005; Milne et al. 2005), and after rising above the present level at around 6.5 ka BP, reaching a maximum level of 2 to 3 m above the present-day level at about 5.5 ka BP (Fig. 10). This was followed either by another

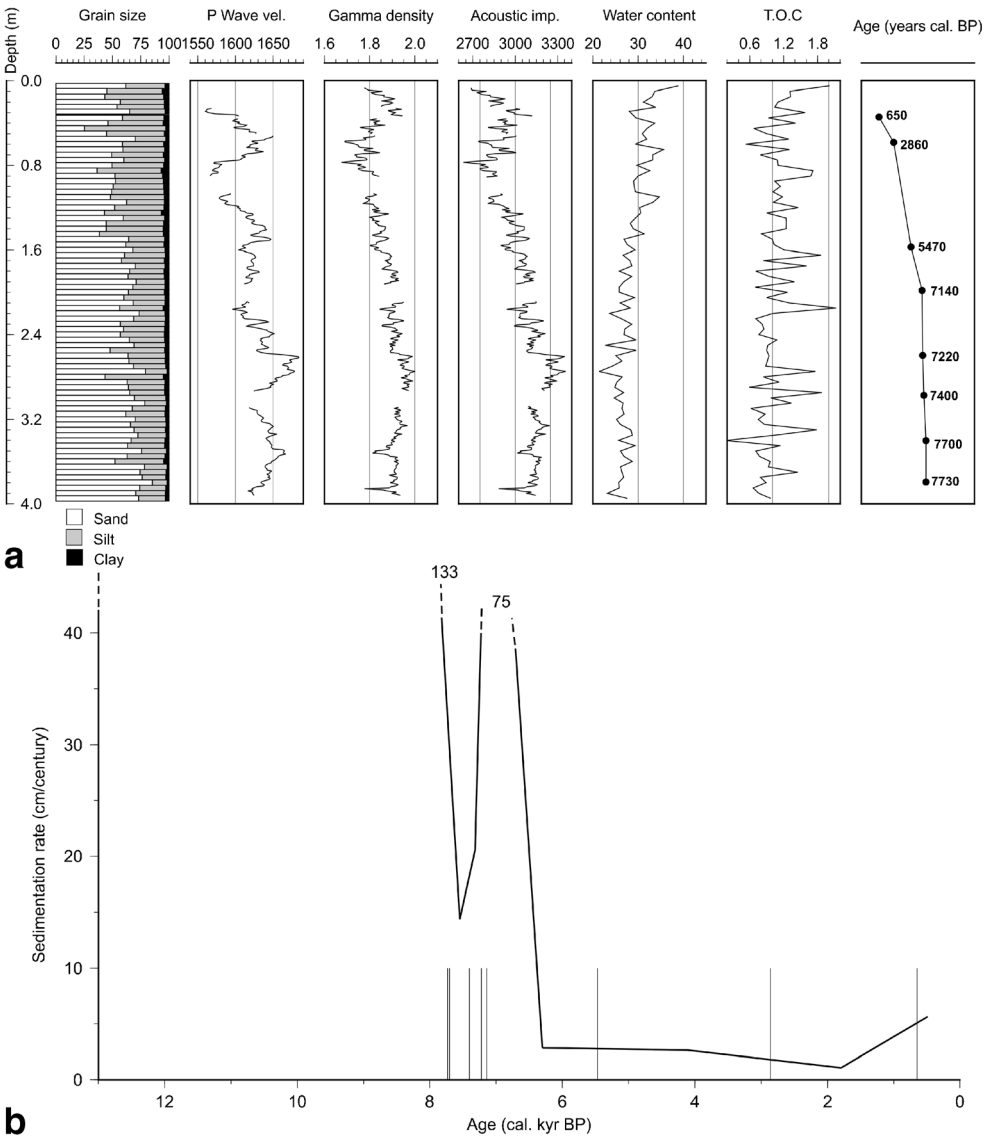

Fig. 8 **a** Downcore profiles for core KCF10-15A (88 m water depth): sand/silt/clay contents (%), P-wave velocity (m s^{-1}), gamma-ray density (g cm^{-3}), acoustic impedance (N s m^{-3}), water content (%), total organic carbon (TOC, %), and ages (cal. years BP). **b** Sedimentation rates over time. *Blue line* Mid-points of individual age intervals, *vertical gray lines* time slices for which AMS ages are available

two high-frequency oscillations (Martin et al. 2003) or by a continuous drop to the present-day level (Cavallotto et al. 2004; Angulo et al. 2006), the evidence in this respect being contradictory.

The second time slice, around approximately 6 ka BP, is represented in all four cores. In this period, an extensive portion of the shelf was now submerged, and the offshore coring site (KCF10-01B) received increasingly less sand and more finer-grained sediment. Sites KCF10-04A and KCF10-09A, which are located on the mid-shelf at water depths of 112 and 110 m respectively, are dominated by fine-grained sediments from the base upward. Correspondingly, the Vp, gamma-ray density and acoustic impedance values are lower than those in the other cores (Figs. 6a, 7a). The Vp values are consistent with the results of Macedo et al. (2009) for the wider study area, and those of, for example, Hamilton (1980) and Richardson and Briggs (2004) for other world regions. As expected, these cores display the highest TOC and water contents of all four cores examined in this study. High TOC contents in low-density sediments have been found by, for example, Mayer et al. (2002) off Cape Hatteras (USA), consistent with the preferential association of organic matter with mud-rich sediments (e.g., Flemming and Delafontaine 2000).

The stratified echo character associated with these cores supports the interpretation of a low-energy, mud-dominated paleo-shoreface environment. The sedimentation pattern is consistent with the stratified echo signature found by, for example, Hong and Chen (2000) under low-energy conditions on the continental margin of Taiwan. Moreover, Mullins et al. (1979; cf. Damuth and Hayes 1977) observed a similar echo character on abyssal plains. The considerable accumulation of mud in this period (Fig. 9) is reflected in the sedimentation-

Table 5 Sedimentation rates for age intervals in core KCF10-15A from the inner shelf

Age interval (cal. years BP)	Depth interval (m)	Sed. rate (cm/century)
0–650	0–34	5.23
650–2,860	34–60	1.17
2,860–5,470	60–160	2.30
5,470–7,140	160–200	2.39
7,140–7,220	200–260	75.00
7,220–7,400	260–291	21.10
7,400–7,700	291–340	14.00
7,700–7,730	340–380	133.30

rate peaks recorded in both cores (Figs. 6b, 7b). The presence of the beach-rock ridge in the central portion of the study area indicates a period of stable sea level. Although no samples were collected to confirm the origin of this feature, previous studies (Figueiredo and Tessler 2004; Reis et al. 2013) described the micro-relief along the 110 m isobath at the southern limit of the Campos basin as of bioconstructional origin. The ridge may have subsequently acted as a localized sediment trap blocking the bypassing of sediment, but the large

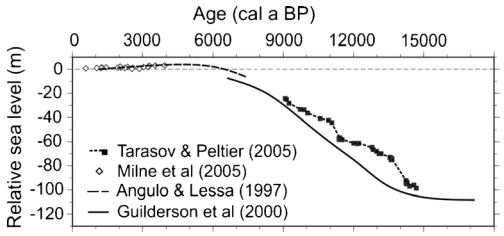

Fig. 10 Sea-level curves for South America reconstructed by Angulo and Lessa (1997), Guilderson et al. (2000), Tarasov and Peltier (2005), and Milne et al. (2005)

sediment thickness northeast of it is more likely related to structural control by the Cabo Frio High.

Sedimentation at the inshore coring site (KCF10-15A) commences at about 7.7 ka BP at its base, the lower half of the core recording extremely high sedimentation rates (Fig. 8a, b), which may at least partially be explained by its proximity to the coast. As sea level rose to its maximum postglacial level, the average sand content gradually decreased from about 75% at the base of the core (7.7 ka BP) to 70% at a core depth of 1.7 m (5.5 ka BP), the overall high sand content explaining the reflective echo character of the seabed.

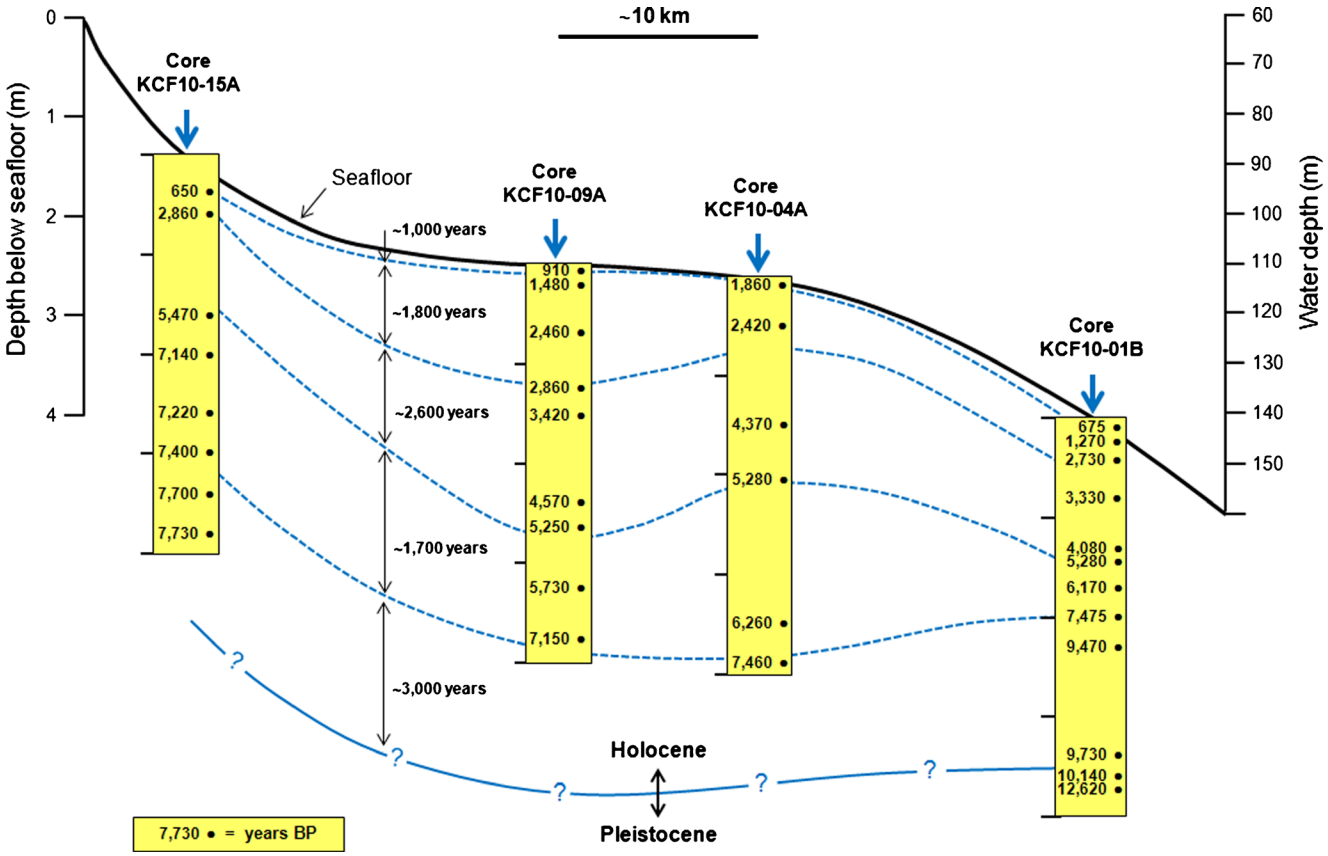

Fig. 9 Cross-section across the shelf with chronostratigraphic tie lines linking individual cores. Note the different age intervals and vertical scales above and below the seafloor

The third time slice represents the period after 3 ka BP, when sea level had more or less reached its present-day position (Corrêa 1996; Fig. 10). Strengthening of the upwelling system led to an increase in productivity (Gyllencreutz et al. 2010). Together with the increasing deposition of finer-grained sediment, this led to higher organic matter contents in the sediment. This applies to all four coring sites, a similar trend having also been reported from the eastern Brazilian shelf by Dominguez et al. (2013).

Millennium-scale sedimentary evolution

The Cabo Frio High probably controlled the planform of the regional coastline ever since its formation. The NW–SE alignment of the beach-rock ridge (Fig. 3) suggests that, in contrast to the present-day E–W orientation (west of Cabo Frio), the coast was oriented NW–SE during the LGM sea-level lowstand. Similar situations along the Brazilian coastline have previously been described by Angulo (1992) and Barbosa (1995).

In his general analysis of eustatic variations along the eastern Brazilian margin, Vieira (1981) identified cyclonic and anti-cyclonic vortices in the Cabo Frio region, which evidently influenced local sedimentation patterns. Thus, hydrostatic pressure differences induce downwelling, in the course of which suspended sediment is trapped in the gyre from where it is deposited on the seabed. This explains the fine-grained nature of the sediment in the mid-shelf cores (KCF10-04A and KCF10-09A; Figs. 6a, 6b, 7a, 7b, and 9).

As observed in the study area today, wave-dominated shallow marine sedimentation influenced by microtidal regimes is sensitive to wave-induced fluctuations in water levels (Davis and Hayes 1984), waves breaking at an angle to the shoreline amplifying alongshore sediment transport. The current pattern at Cabo Frio is complex because of the interaction between the shelf front caused by the upwelling of South Atlantic Central Water in the wake of intrusions of the Brazil Current, and seasonal wind- or storm-induced coastal currents that converge on Cabo Frio from the west and northeast. At Cabo Frio the coastal currents are deflected offshore toward the southeast (Viana et al. 1998; Piola et al. 2000; Belem et al. 2013). The intruding Brazil Current slows the offshore-directed currents (Mesquita and Harari 2000), causing their suspended load to be deposited across the shelf (Fig. 11). In addition, this shear stress model results in the formation of sand ridges on the shoreface near the coast (Figueiredo 1980). In general, the coastal currents, in which the frictional coupling between wind and fluid causes the water to be driven forward, have a large capacity for sediment transport (Walker and Plint 1992). The existence of such mechanisms in the past is also supported by the chronological inversions found in some of the strata (Table 1).

Cores KCB10-01B and KCF10-15A, i.e., the inner and outer shelf cores, exhibit very similar sedimentological sequences and acoustic patterns associated with coarse material, suggesting that

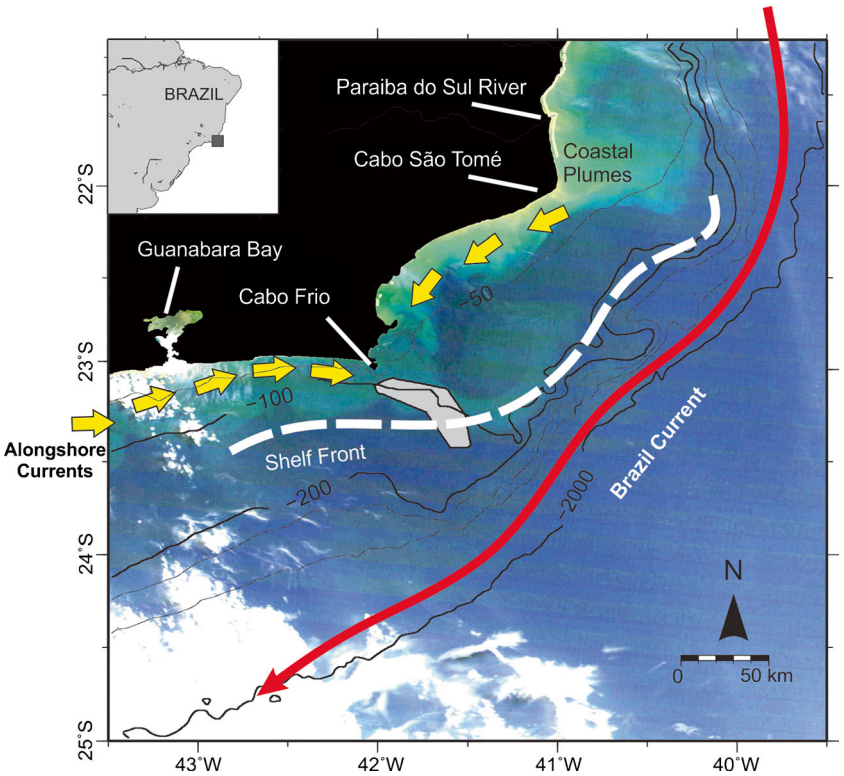

Fig. 11 Schematic representation of the interaction between the Brazil Current and the inshore coastal countercurrent, which is deflected offshore at Cabo Frio. The reduction in velocity associated with the shelf front caused by the intrusion of South Atlantic Central Water at the bottom results in the spatially confined cross-shelf accumulation of sediment (background image: MODIS Aqua TrueColor, EOSDIS-NASA, 21 June 2008)

both are endmembers of the same basic sedimentation model, in which wind- and wave-driven alongshore transport of bedload material is deflected by a change in shoreline orientation to result in a similar depositional pattern, albeit at different times. This pattern suggests that the source of terrigenous sand may have been a barrier-island complex, which initially developed during the LGM and that was subsequently displaced landward in the course of sea-level rise until it stabilized some 6.5 ka BP along the modern coast (Turcq et al. 1999). That terrigenous sand can be transported far offshore on the shelf off SE Brazil was already noted by Summerhayes (1976) and more recently confirmed by Gyllencreutz et al. (2010). At the same time, muddy suspended sediment derived from Guanabara Bay and the discharge of the Paraiba do Sul and smaller rivers was transported to the area by longshore drift (Dominguez et al. 1987, 2013) to be deposited further offshore in the enigmatic cross-shore depocenter to the southeast of Cabo Frio (Viana et al. 1998).

In conclusion, further core-based studies are required to better define the regional Pleistocene–Holocene transition of the shelf sediments off Cabo Frio. In particular, the nature of the lower sedimentation unit deserves further attention—all that is currently known about this unit is that it must be of Pleistocene age. This could be achieved by collecting cores on a lateral transect along which the upper sedimentation unit thins out.

Acknowledgements This work was funded by the Geochemistry Network of PETROBRAS/CENPES and the Brazilian National Petroleum and the Biofuels Agency (ANP). We thank Dr. Marcio Gurgel for collecting the samples. We also wish to acknowledge constructive reviews by R. Gyllencreutz and T. Mulder as well as additional comments by the editors, all of which helped improve the final paper.

References

Anderson TW, Finn JD (1996) The new statistical analysis of data. Springer, New York

Angulo RJ (1992) Geologia da planície costeira do Estado do Paraná. Dissertation, University of São Paulo

Angulo RJ, Lessa GC (1997) The Brazilian sea-level curves: a critical review with emphasis on the curves from the Paranaguá and Cananéia regions. Mar Geol 140:141–166

Angulo RJ, Souza MC, Reimer PJ, Sasaoka SK (2005) Reservoir effect of the southeastern Brazilian coast. Radiocarbon 47:67–73

Angulo RJ, Lessa GC, Souza MC (2006) A critical review of mid- to late-Holocene sea-level fluctuations on the eastern Brazilian coastline. Quat Sci Rev 25:486–506

Artusi L, Figueiredo AG Jr (2007) Sismoestratigrafia rasa da plataforma continental de Cabo Frio - Arraruama - RJ. Rev Bras Geofis 25:7–16

Barbosa CF (1995) Foraminifera e Arcellacea ("Thecamoebia") recentes do estuário de Guaratuba, Paraná Brasil. An Acad Bras Ciênc 67: 465–492

Barbosa CF (1997) Reconstituicão paleoambiental de fácies lagunares com base em foraminiferos: o nível do mar no Quaternário Superior na área de Cabo Frio. Dissertation, University of São Paulo

Barbosa CF, Suguio K (1999) Bio-sedimentary facies of a subtropical microtidal estuary - an example from southern Brazil. J Sediment Res 69:576–587

Bard E, Arnold M, Hamelin B, Tisnerat-Laborde N, Cabioch G (1998) Radiocarbon calibration by means of mass spectrometric $^{230}Th/^{234}U$ and ^{14}C ages of corals. An update data base including samples from Barbados, Mururoa and Tahiti. Radiocarbon 40:1085–1092

Belem AL, Castelao RM, Albuquerque ALS (2013) Controls of subsurface temperature variability in a western boundary upwelling system. Geophys Res Lett 40:1362–1366

Blott S, Pye K (2001) Gradistat: a grain-size distribution and statistics package for the analysis of unconsolidated sediments by sieving or laser granulometer. Earth Surf Process Landf 26:1237–1248

Briggs KB, Williams KL, Jackson DR, Jones CD, Ivakin AN, Orsi TH (2002) Fine scale sedimentary structure: implications for acoustic remote sensing. Mar Geol 182:141–159

Castelao RM, Barth JA (2006) Upwelling around Cabo Frio, Brazil: the importance of wind stress curl. Geophys Res Lett 33, L03602. doi: 10.1029/2005GL025182

Castro BM, Miranda LB (1998) Physical oceanography of the western Atlantic continental shelf located between 4°N and 34°S. In: Robinson AR, Brinks KH (eds) The sea. Wiley, New York, pp 209–251

Cavallotto JL, Violante RA, Parker G (2004) Sea-level fluctuations during the last 8600 years in the de la Plata river (Argentina). Quat Int 114:155–165

Corrêa ICS (1990) Analyse morphostructurale et évolution paléogéographique de la plate-forme continentale Atlantique sud-brésilienne (Rio Grande do Sul – Brésil). Dissertation, University of Bordeaux I

Corrêa ICS (1996) Les variations du niveau de la mer durant les derniers 17.500 ans BP: l'exemple de la plate-forme continentale du Rio Grande do Sul-Brésil. Mar Geol 130:163–178

Cruz APS, Barbosa CF, Ayres-Neto A, Albuquerque ALS (2013) Physical and geochemical properties of centennial marine sediments of the continental shelf of southeast Brazil. Geochim Bras 27(1):1–12

Damuth JE (1975) Quaternary climate change as revealed by calcium carbonate fluctuations in western Equatorial Atlantic sediments. Deep-Sea Res 22:725–743

Damuth JE, Hayes DE (1977) Echo character of the east Brazilian continental margin and its relationship to sedimentary processes. Mar Geol 24:73–95

Davis RA, Hayes JD (1984) What is a wave-dominated coast? Mar Geol 60:313–329

Davis A, Haynes R, Bennell B, Huws D (2002) Surficial seabed sediment properties derived from seismic profiler responses. Mar Geol 182: 209–223

Dias GTM, Palma JJC, Ponzi VRA (1982) Matéria orgânica no Quaternário da margem continental entre Rio de Janeiro e Guarapari. LAGEMAR/PETROBRAS/CENPES, Rio de Janeiro, Brazil

Dominguez JML, Martin L, Bittencourt ACSP (1987) Sea-level history and the Quaternary evolution of river mouth-associated beach-ridge plains along the east-southeast coast of Brazil: a summary. In: Nummedal D, Pilkey OH, Howard JD (eds) Sea-level fluctuation and coastal evolution. SEPM Spec Publ 41:115–127

Dominguez JML, da Silva RP, Nunes AS, Freire AFM (2013) The narrow, shallow, low-accommodation shelf of central Brazil: sedimentology, evolution, and human uses. Geomorphology 203:46–59

Figueiredo AG Jr (1980) Response of water column to strong wind forcing, southern Brazilian inner-shelf: implications for sand ridge formation. Mar Geol 35:367–376

Figueiredo AG Jr, Madureira LSP (2004) Topografia, composição, refletividade do substrato marinho e identificação de províncias sedimentares da região Sudeste-Sul do Brasil. Technical Report, Série Documentos Técnicos do Programa REVIZEE Score-Sul, Instituto Oceanográfico - USP, São Paulo, pp 46–55

Figueiredo AG Jr, Tessler MG (2004) Topografia e composição do substrato marinho da região Sudeste-Sul do Brasil. Technical Report, Série Documentos Técnicos do Programa REVIZEE Score-Sul, Instituto Oceanográfico - USP, São Paulo, pp 56–64

Flemming BW, Delafontaine MT (2000) Mass physical properties of muddy intertidal sediments: some applications, misapplications and non-applications. Cont Shelf Res 20:1179–1197

Franchito SH, Oda TO, Brahmananda RV, Kayano MT (2008) Interaction between coastal upwelling and local winds at Cabo Frio, Brazil: an observational study. J Appl Meteorol Climatol 47:1590–1598

Guilderson TP, Burckle L, Hemming S, Peltier WR (2000) Late Pleistocene sea level variations derived from the Argentine Shelf. Geochem Geophys Geosyst 1:1055. doi:10.1029/2000GC000098

Gyllencreutz R, Mahiques MM, Alves DVP, Wainer IKC (2010) Mid- to late-Holocene paleoceanographic changes on the southeastern Brazilian shelf based on grain-size records. The Holocene 20:863–875

Hamilton EL (1980) Geoacoustic modeling of the sea floor. J Acoust Soc Am 68:1313–1336

Hong E, Chen IS (2000) Echo characters and sedimentary processes along a rifting continental margin, northeast of Taiwan. Cont Shelf Res 20:599–617

Knoppers B, Moreira PF (1990) Matéria em suspensão e a sucessão do fito plâncton na Lagoa de Guarapina, RJ. Acta limnol Bras 3:291–317

Kowsmann RO, Costa MPA (1979) Sedimentação Quaternária da margem continental brasileira e das áreas oceânicas adjacentes. In: Projeto REMAC – Reconhecimento Global da margem continental brasileira. PETROBRAS/CENPES/DINTEP/CPRM/DHN/CNPq, Rio de Janeiro, pp 9–55

Krumbein WC, Pettijohn FJ (1988) Manual of Sedimentary Petrology. Society of Economic Paleontologists and Mineralogists. Tulsa, OK

Lambeck K, Chappell J (2001) Sea level change through the Last Glacial Cycle. Science 292:679–686

Macedo HC, Figueiredo AG, Machado JC (2009) Propiedades acústicas (velocidade de propagação e coeficiente de atenuação) de sedimentos marinhos coletados nas proximidades da ilha de Cabo Frio, RJ. Rev Bras Geofis 27:195–204

Mahiques MM, da Silveira ICA, Souza SHM, Rodrigues M (2002) Post-LGM sedimentation on the outer-shelf – upper slope of the northernmost part of the São Paulo Bight, southeastern Brazil. Mar Geol 181:387–400

Mahiques MM, Tessler MG, Ciotti AM, da Silveira IC, Sousa SHM, Figueira RCL, Tassinari CCG, Furtado VV, Passos RF (2004) Hydrodynamically driven patterns of recent sedimentation in the shelf and upper slope off Southeast Brazil. Cont Shelf Res 24:1685–1697

de Mahiques MM, Bícego MC, da Silveira ICA, Sousa SHM, Lourenço RA, Fukumoto MM (2005) Modern sedimentation in the Cabo Frio upwelling system, southeastern Brazilian shelf. An Acad Bras Ciên 77(3):535–548

de Mahiques MM, Wainer IKC, Burone L, Nagai R, de Mello e Sousa SH, Figueira RCL, da Silveira ICA, Bícego MC, Alves DPV, Hammer Ø (2009) A high-resolution Holocene record on the southern Brazilian shelf: paleoenvironmental implications. Quat Int 206:52–61

Mahiques MM, Sousa SHM, Burone L, Nagai RH, da Silveira ICA, Figueira RCL, Soutelino RG, Ponsoni L, Klein DA (2011) Radiocarbon geochronology of the sediments in the São Paulo Bight (southern Brazilian upper margin). An Acad Bras Ciên 83(3):817–834

Manley PL, Flood RD (1989) Anomalous sound velocities in near surface, organic rich, gassy sediments in the central Argentine Basin. Deep-Sea Res 36:611–623

Martin L, Dominguez JML, Bittencourt ACSP (2003) Fluctuating Holocene sea-levels in eastern and southeastern Brazil: evidence from multiple fossil and geometric indicators. J Coast Res 19:101–124

Mayer L, Benninger L, Bock M, DeMaster D, Roberts Q, Martens C (2002) Mineral associations and nutritional quality of organic matter in shelf and upper slope sediments off Cape Hatteras, USA: a case of unusually high loadings. Deep-Sea Res II 49:4587–4597

Mesquita AR, Harari J (2000) On the sea-level network and circulation in the southeastern Brazilian coast. IOC/UNESCO WSR 171:46–63

Milne GA, Long AJ, Bassett SE (2005) Modelling Holocene relative sea-level observations from the Caribbean and South America. Quat Sci Rev 24:1183–1202

Mullins HT, Boardman MR, Neumann AC (1979) Echo character of off-platform carbonates. Mar Geol 32:251–268

Nagai RH, Sousa SHM, Burone L, Mahiques MM (2009) Paleoproductivity changes during the Holocene in the inner-shelf of Cabo Frio, southeastern Brazilian continental margin: benthic foraminifera and sedimentological proxies. Quat Int 206:62–71

Omura A, Hoyanagi K (2004) Relationships between composition of organic matter, depositional environments, and sea-level changes in backarc basins, central Japan. J Sediment Res 74:620–630

Petrocelli BT (2013) Processamento sísmico aplicado a dados de alta resolução para caracterização de feição geológica do fundo oceânico ao largo de Cabo Frio-RJ. PhD Thesis, Universidade Federal Fluminense, Niterói, RJ

Piola AR, Campos EJD, Moller OO, Charo M, Martinez C (2000) Subtropical shelf front off eastern South America. J Geophys Res 105:6566–6578

Reis AT, Maia RMC, Silva CG, Rabineau M, Guerra JV, Corini C, Ayres A, Arantes-Oliveira R, Benabdellouahed M, Simões I, Tardin R (2013) Origin of step-like and lobate seafloor features along the continental shelf off Rio de Janeiro State, Santos basin-Brazil. Geomorphology 203:25–45

Richardson MD, Briggs KB (2004) Empirical predictions of seafloor properties based on remotely measured sediment impedance. In: Siderius M, Kuperman WA, Porter MB (eds) High frequency ocean acoustics. American Institute of Physics, La Joya, CA, pp 12–21

Rodrigues RR, Lorenzzetti JA (2001) A numerical study of the effects of bottom topography and coastline geometry of the Southeast Brazilian coastal upwelling. Cont Shelf Res 21:371–394

Sallun AEM, Sallun Filho W, Suguio K, Babinski M, Gioia SMCL, Harlow BA, Duleba W, De Oliveira PE, Garcia MJ, Weber CZ, Christofoletti SR, da S Santos C, de Medeiros VB, Silva JB, Santiago-Hussein MC, Fernandes RS (2012) Geochemical evidence of the 8.2 ka event and other Holocene environmental changes recorded in paleolagoon sediments, southeastern Brazil. Quat Res 77(1):31–43

Sanders CJ, Caldeira PP, Smoak JM, Ketterer ME, Belem A, Mendoza UMN, Cordeiro LGMS, Silva-Filho EV, Patchineelam SR, Albuquerque ALS (2014) Recent organic carbon accumulation (100 years) along the Cabo Frio, Brazil upwelling region. Cont Shelf Res 75:68–75

Sawakuchi AO, Giannini PCF, Martinho CT, Tanaka APB (2009) Grain-size and heavy minerals of the Late Quaternary eolian sediments from the Imbituba-Jaguaruna coast, Southern Brazil: depositional controls linked to relative sea-level changes. Sediment Geol 222:226–240

Souto DD, Lesa DO, Albuquerque AS, Sifeddine A, Turcq BJ, Barbosa CF (2011) Marine sediments from southeastern Brazilian continental shelf: a 1200 year record of upwelling productivity. Palaeogeogr Palaeoclimatol Palaeoecol 299:49–55

Stuiver M, Reimer PJ, Bard E, Burr GS, Hughen KA, Kromer B, McCormac GVD, Plicht J, Spurk M (1998) INTCAL98 Radiocarbon Age Calibration. Radiocarbon 40:1041–1083

Summerhayes CP (1976) The influence of upwelling on suspended matter and shelf sediments off southeastern Brazil. J Sediment Petrol 46:819–828

Swan D, Clague JJ, Luternauer JL (1979) Grain-size statistics II: evaluation of grouped moment measures. J Sediment Petrol 49:487–500

Tarasov L, Peltier WR (2005) Arctic freshwater forcing of the Younger Dryas cold reversal. Nature 435:662–665

Turcq B, Martin L, Flexor JM, Suguio K, Pierre C, Tasayaco-Ortega L (1999) Origin and evolution of the Quaternary coastal plain between Guaratiba and Cabo Frio, State of Rio de Janeiro, Brazil. In: Knoppers B, Bidone ED, Abrão JJ (eds) Environmental geochemistry of coastal lagoon systems. Série Geoquímica Ambiental, Niterói, RJ, pp 25–46

Viana AR, Faugères J-C, Kowsmann RO, Lima JAM, Caddah LEG, Rizzo JG (1998) Hydrology, morphology and sedimentology of the Campos continental margin, offshore Brazil. Sediment Geol 115:133–157

Vieira PC (1981) Variacões do nivel marinho: alterações eustaticas no Quaternário. Rev Inst Geociên 2:39–58

Walker RG, Plint AG (1992) Wave- and storm-dominated shallow marine systems. In: Walker RG, James NP (eds) Facies models response to sea-level change. Geological Association of Canada, St. John's, NL, pp 219–238